MODELING OF DROPLET MOTION ON TEXTURED SURFACES

A THESIS SUBMITTED TO

THE GRADUATE SCHOOL OF ENGINEERING AND SCIENCE

OF BILKENT UNIVERSITY

IN PARTIAL FULFILLMENT OF THE REQUIREMENTS FOR

THE DEGREE OF

MASTER OF SCIENCE

IN

MECHANICAL ENGINEERING

By

Mayssam Naji

September 2021

Modeling of Droplet Motion on Textured Surfaces

By Mayssam Naji

September 2021

We certify that we have read this thesis and that in our opinion it is fully adequate, in scope and in quality, as a thesis for the degree of Master of Science.

Yegan Erdem(Advisor)

Ali Javili

Mustafa Ünel

Approved for the Graduate School of Engineering and Science:

Ezhan Karaşan
Director of the Graduate School

ABSTRACT

MODELING OF DROPLET MOTION ON TEXTURED SURFACES

Mayssam Naji
M.S. in Mechanical Engineering
Advisor: Yegan Erdem
September 2021

We describe the motion of a droplet on a textured ratchet track using a non-linear resonator model. A textured ratchet track is composed of semi-circular pillar array that induces a net surface tension gradient on a droplet placed on it. When a vertical vibration is applied, hysteresis is overcome, and the droplet moves towards the local lower energy barrier; however, due to the repetitive structure of texture, it keeps moving until the end of the track. The droplet motion depends on the amplitude and frequency of the vertical oscillation, and this dependence is nonlinear. Therefore, finding a fully analytical solution to represent this motion is not trivial. Consequently, the droplet motion still remains as a topic that needs further investigation. In this study we elaborate on the utility of double-pendulum as a basis for modeling the droplet motion on surfaces. Similar to the droplet motion, resonators, such as double pendulum, are simple, yet non-linear systems. Moreover, inverted double pendulum motion has key characteristics such as two phase motion and double peak motion, which are also observed in the droplet motion on textured ratchets. In this thesis, data processing models are developed to highlight the similarity between these two systems both qualitatively and quantitatively. After establishing this comparison, a model is proposed that utilizes an inverted double pendulum mounted on a moving cart to successfully simulate the motion of a droplet on a ratchet track. This methodology will lead to developing an accurate droplet-motion modeling approach which will be useful to understand droplet dynamics in more depth.

Keywords: Droplet Motion, Numerical Modeling, Ratchet Tracks, Double Pendulum, Parametric Oscillator.

ÖZET

DOKULU YUZEYLERDE DAMLACIK HAREKETI MODELLEMESI

Mayssam Naji
Makine Mühendisliği, Yüksek Lisans
Tez Danışmanı: Yegan Erdem
Eylül 2017

Bu tezde doğrusal olmayan bir rezonatör modeli kullanarak dokulu bir mandal üzerindeki bir damlacık hareketi açıklanmaktadır. Dokulu mandal, üzerine yerleştirilen bir damlacık üzerinde net yüzey gerilim gradyanı oluşturan yarı dairesel sütun dizisinden oluşur. Dikey bir titreşim uygulandığında, histerezis aşılır ve damlacık yerel düşük enerji bariyerine doğru hareket eder; ancak, dokunun tekrarlayan yapısı nedeniyle, pistin sonuna kadar hareket etmeye devam eder. Damlacık hareketi dikey salınımın genliğine ve frekansına bağlıdır ve bu bağımlılık doğrusal değildir. Bu nedenle, bu hareketi temsil etmek için tamamen analitik bir çözüm bulmak önemsiz değildir. Sonuç olarak, damlacık hareketi hala daha fazla araştırılması gereken bir konu olarak kalmaktadır. Bu çalışmada, yüzeylerdeki damlacık hareketini modellemek için bir temel olarak çift sarkaçın faydasını detaylandırıyoruz. Damlacık hareketine benzer şekilde, çift sarkaç gibi rezonatörler basit ancak doğrusal olmayan sistemlerdir. Ayrıca, ters çift sarkaç hareketi, dokulu cırcırlardaki damlacık hareketinde de gözlenen iki faz hareketi ve çift tepe hareketi gibi temel özelliklere sahiptir. Bu tezde, bu iki sistem arasındaki benzerliği hem niteliksel hem de niceliksel olarak vurgulamak için veri işleme modelleri geliştirilmiştir. Bu karşılaştırmayı oluşturduktan sonra, bir mandal yolundaki bir damlacık hareketini başarıyla simüle etmek için hareketli bir arabaya monte edilmiş ters bir çift sarkaç kullanan bir model önerilmektedir. Bu metodoloji, damlacık dinamiklerini daha derinlemesine anlamak için yararlı olacak doğru bir damlacık hareket modelleme yaklaşımı geliştirmeyi sağlayacaktır.

Anahtar sözcükler: Damlacık Hareketi, Sayısal Modelleme, Cırcır İzleri, Çift Sarkaç, Parametrik Osilatör.

Acknowledgement

I would like to thank Professor Yegan Erdem, for her continuous support. She was not only my advisor and mentor but also a major inspiration for career.
Further, I would like to thank the committee members of this thesis, to Professor Mustafa Ünel and Professor Ali Javili for their time, and their valuable feedback.
I want to thank to all members of Micro and Nano Integrated Fluids (MiNI) Research Group, Ecem Yelekli, Berkay Şahinoğlu, Malik Abdul Wahab, Eliza Sopubekova, Gökçe Özkazanç, Büşra Sarıarslan, Muhammad Saqib, for their help and support.
I would like to thank my Family, Diaa, Souha, Ayda, Yahya, and Nur for their unconditional love. And specially my Grandmother, Faiza, for supporting me in the most difficult times.
Finally, I am forever to be thankful for my Bilkent family, Youssef Tekriti, Sarjeel Yusuf, Anooshay Khan, Salman Mohammad, Yassin Elamin, Suzan Hamed, Leyla Khasiyeva, Helin Hocaoğlu, Selina Hajarat, Gül Karakuş, Javaid Jabbar, and many other Bilkent individuals to whom I will be forever grateful.
This work would not have been possible without the support of The Scientific and Technological Research Council of Turkey (TUBITAK) under the grant number 117M492

Contents

List of Figures

List of Tables

Chapter 1

Introduction

The ability to control fluid flow in micro scales favors successful applications in single-cell analysis, biochemistry, and diagnostics which has also induced a growing interest in the understanding of droplet motion in detail. Fully integrated devices for biomedical and chemical applications were brought to life as a result of the advancement in microfluidics technology [1, 2, 3, 4, 5, 6, 7, 8] and the ability to control individual droplets of samples [9, 10, 11, 12]. The applications vary across a wide range, such as elimination of cross-contamination, rapid mixing, reduced material usage, and better concentration control [13]. Droplet manipulation can take place in microchannels of Lab On Chip (LOC) devices [14]. In the first method, droplets are manipulated in an immiscible continuous fluid inside a microchannel. The second type is that of an open system, in which the droplet moves freely often on a hydrophobic surface in the open air[15]. Manipulation of droplets on surfaces has many advantages including delicate control of the motion, prevention of the dilution of the droplet which is usually caused across the two-phase boundary by either diffusion or contamination; and eliminations of complications such as clogging and leakages [16].
The method relies on a surface energy gradient to achieve directional droplet propagation. This gradient can be generated in several ways such as electrowetting, super para-magnetism, Leidenfrost effect, or surface texture[17]. Few models were developed to recreate the mechanisms of droplet motion of the previous

systems. Goohpattader et al.[18] proposed a model of a sphere on a patterned substrate in a drift during stochastic rolling. Daniel[19], Buguin[20], Mettu[21], and their research teams were able to describe the horizontal vibration seen in droplet motion by vanquishing the contact angle hysteresis, resulting in a net droplet motion. Noblin's model described that the interplay between horizontal and vertical vibrations is the cause of the force asymmetry and hence a net droplet motion [22]. Agapov et al. and Malvadkar et al. showed the droplet transport with micro and nanostructured tilted pillars by the pin-release mechanism of a ratchet, which they achieved by analyzing contact angles at micron scale[23, 24]. Moreover, Sekeroglu et al.analyzed the droplet motion on microgels and the effect of added mass [25] . A more analytical method was proposed by Chamakos et al., which is the finite element method to describe the droplet motion on super-hydrophobic surfaces with the asymmetric textured and It was further developed by Tretyakov and Muller by using the molecular dynamic [26, 27].

In order to manipulate the motion of droplets on surfaces, few methods were used, and what was proposed in this thesis was the droplet manipulation achieved by creating energy gradients with surface texture. In this model, the surface is made of a textured pattern enabling the wetting and dewetting [28] which mechanism was studied carefully and a physical model for its physics was proposed. The method was first introduced by Shastry et al, in which pillar arrays with a vertical vibration were used for the droplet to overcome hysteresis [29]. The pillar arrays create an asymmetric surface force at the three-phase contact of the droplet [30]. Moreover, the work done by many research groups is investigated to draw the relation between the parameters(frequency and amplitude), and droplet properties such as volume and chemical composition [31, 32, 30, 33, 29]. The theoretical work covering the mechanism of the droplet's motion is well explored by few researchers notably Shastry et al. and Duncombe et al., and not as much as the complexity of this non-linear behavior needs [29, 30]. The latter is due to the complication of providing such an accurate framework that is able to reproduce the motion of droplets in such conditions. The theoretical works have been directed into the field of modeling droplet-surface interaction such as droplet-imprint shape [34, 35] and the mass-spring-damper system which is explored in section 1.5 [32].

The model proposed in this thesis is primarily an analytical approach. The motion of the double pendulum on a cart is developed by studying its key features with respect to the droplet motion. First, droplet motion on a ratchet track is studied and observations were made to understand its nonlinear behavior. Secondly, a model for a double pendulum mounted on a cart is developed to determine its resemblance to the droplet motion. This resemblance is studied by using the Elastic Functional Data Analysis (EFDA) and comparing the model with the experimental data using Frechet Distance. To acquire the experimental data, the motion of the water droplet on the ratchet track is recorded with a high-speed camera. The theoretical framework aimed to understand the motion of the droplet on tracks is of great importance for understanding its potential in microfluidic applications. In this chapter, the key features of the droplet motion is explained along with an introduction to the wetting phenomena, different states of droplet motion, and manipulation techniques.

1.1 Wetting in Nature

Wetting is the spread of liquid on a surface that is solid or liquid, and it is an important phenomena to understand liquid behavior in nature and industrial applications such as painting, treatment of automobile tires for enhancement of adhesion to icy roads, production of anti-frost glasses, and waterproof concrete for construction [36]. In nature, few creatures apply the wetting characteristics for survival, such as Namib desert beetle that is able to capture water from the fog [37].In addition, shorebirds can feed themselves by transporting their prey inside the droplets coming for their beak to their mouth in a step Ratchet manner [38]. The application of the wetting phenomena is wide and can be seen in the water transportation of plants from their roots to their leaves, and the motion of insects on the surface of liquid water [39]. Few of the superhydrophobic surfaces can have high contact angle hysteresis e.g. leaves of scallion and garlic. On these leaves, the water droplets are larger than 150°angle when the leaves are titled vertically, the water droplets do not drop [39]. The latter is an essential feature for few plants in keeping them hydrated. Few plants have superhydrophilic surfaces for photosynthesis. Termites use hydrophilic parts of their body ad wings to spread the places with large quantities of water, which helps with their colonization [37]. Characteristics of the wetting phenomena are well studied due to their potential in a wide application spectrum as in self-cleaning, anti-fogging, droplet manipulation, oil-water separation, anti-fouling, printing techniques, optical devices, and the lab on chip applications and microfluidic devices. The only way to have a deeper understanding is to have a keen observation of this phenomenon in nature and to try mimicking it, as explored in the next section

1.2 Theoretical Background

Wetting, theoretically, is a thermodynamic process conditioned by the surface energy balance at the interfaces. When liquid makes contact with a solid surface, the air-solid interface is replaced by the liquid-solid interface, and eventually, a new liquid-air interface is formed, resulting in three interfaces: liquid-solid, solid-air, liquid-air as in Figure 1.1.

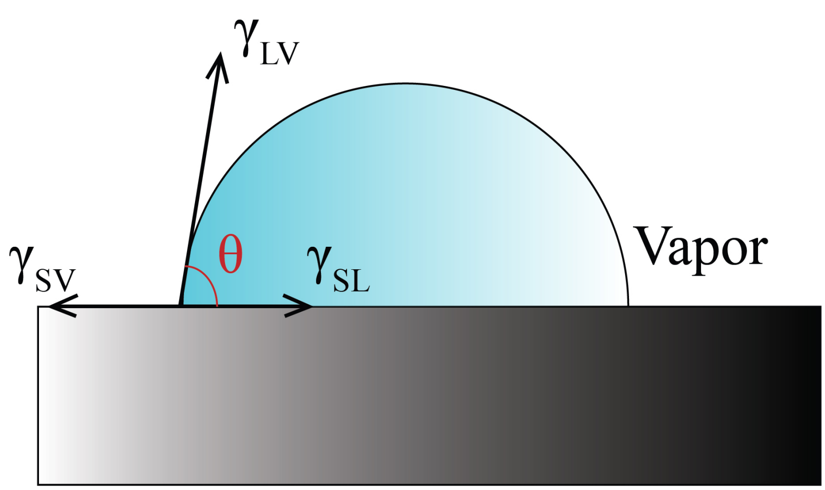

Figure 1.1: Liquid droplet on the solid substrate forming a contact angle θ resulting from the surface forces in balance

The total energy of the system can either decrease or increase when a new surface forms as each interface has its own energy. The total energy determines the wetting behavior of the system. The contact angle and its hysteresis identify this property [39]. The static contact angle is the angle between the tangent of the liquid-gas interface and the tangent of the solid-liquid interface and varies between $0°$ to $180°$ depending on the wetting scale. The variation gives rise to different states from super wetting (complete wetting) for $0°$ contact angle and dewetting for $180°$. The classification of wetting states can be grouped into four, depending on the static contact angle: (a) Hydrophilic state, in which the water droplet makes a contact angle $10° < \theta < 90°$; (b) hydrophobic state, for $90° < \theta < 150°$; (c) Superhydrophilic state, where the water droplet wets the solid surface and has $\theta < 10°$; (d) superhydrophobic state, for $\theta > 150°$, see Figure 1.2 .

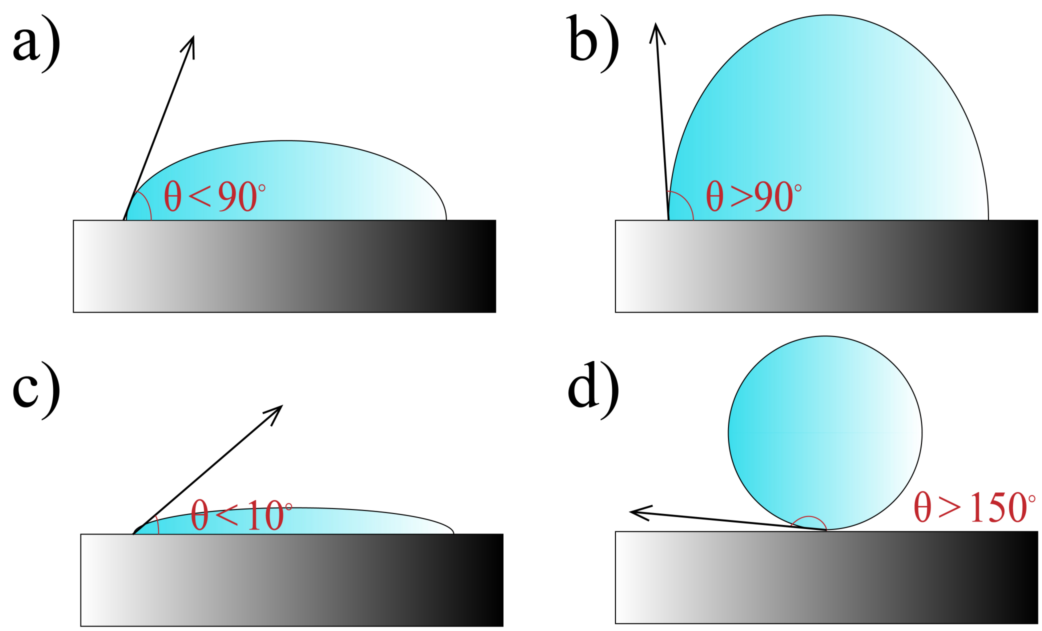

Figure 1.2: The classification of wetting states grouped into four, depending on the static contact angle: (a) Hydrophilic state, $10° < \theta < 90°$; (b) hydrophobic state, for $90° < \theta < 150°$; (c) superhydrophilic state, that has $\theta < 10°$; (d) superhydrophobic state, for $\theta > 150°$.

Another feature to describe the wettability is the contact angle hysteresis. It can be defined by the difference between the advancing angle θ_{adv} which is the maximum contact angle the droplet can attain and between the receding contact angle θ_{rec} which is the lowest possible contact angle that the droplet can have on the surface. The main factor playing role in this hysteresis is the pinning forces, which result from the roughness, physical/chemical heterogeneity, and defects on the surface. This gains more importance when the droplet is in motion. When the contact angle hysteresis is large, the energy required to put the droplet into motion is larger, whereas, when the hysteresis is small enough, the droplet is mobile and can roll with smaller forces in the play such as blowing the air or slight tilt in the solid surface. The rolling of droplets can be observed in certain systems in nature which inspired many researchers to design biometric surfaces with such property.

1.3 Effect of Surface Texture on Wetting

1.3.1 Young-Dupré Equation

Young-Dupré equation was derived about 200 years ago and it is essential to understand the wetting [40, 41]. The equation relates the equilibrium contact angle $\theta_E q$ of a droplet on the smooth surface to the surface tension of solid-liquid (γ_{SL}), liquid-gas (γ_{LG}), liquid-gas (γ_{SG}) interfaces:

$$\gamma_{SL} + \gamma_{LG} \cos\theta_{Eq} = \gamma_{SG} \tag{1.1}$$

The previous equation can be derived by showing the forces in play on the droplet as shown in Figure 1.1. Once the surface tension values are known, the wetting angle can be determined from the previous equation. The surface is hydrophobic when the solid-gas interface surface tension is lower than that of the solid-liquid interface. However, this equation does not consider roughness, chemical heterogeneity, defects, swelling, and dissolution [40].

1.3.2 Wenzel's Model

There are two different states the liquid droplet can stay on a rough surface: Wenzel and Cassie-Baxter state. These models are valid when the roughness size is comparably small with respect to the droplet size. Wenzel state is observed when the liquid droplet is completely in contact with the rough surface.

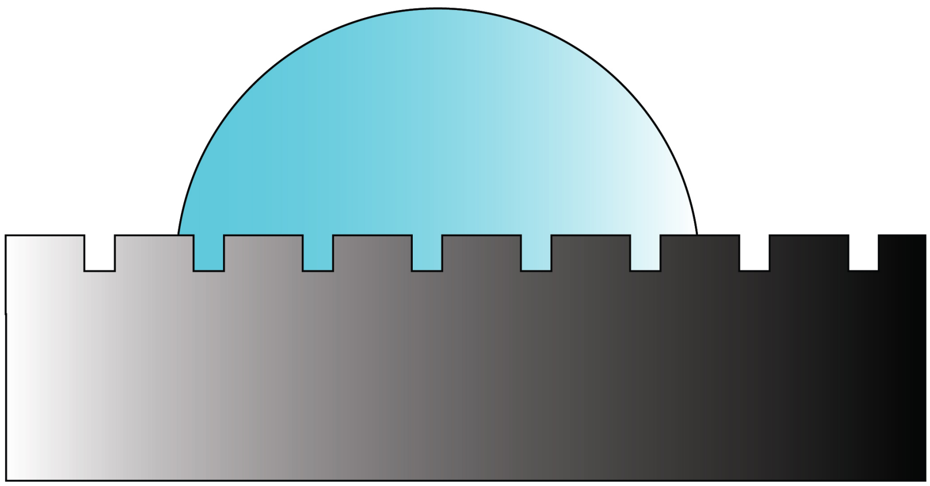

Figure 1.3: Wenzel state, where the liquid droplet is completely in contact with the rough surface.

The apparent contact angle can be calculated by the following Wenzel model, on a rough and chemically homogeneous surface:

$$\cos\theta^* = r\cos\theta_{Eq} \tag{1.2}$$

θ_{Eq} being the contact angle on the flat surface (Young-Dupré angle), r the surface roughness, and θ^* the apparent contact angle on the rough surface. Roughness is the ratio of surface area to the projected surface area. As shown in the equation above, the apparent contact angle becomes larger ($\theta^* \gg 90^{\circ}$) when the apparent contact angle θ is larger than 90° ($\theta_{Eq} > 90^{\circ}$) and vice versa. Therefore, the wetting properties are maximized or minimized with the roughness. In other words, it makes the hydrophobic surface more hydrophobic.

1.3.3 Cassie-Baxter Model

Cassie Baxter's state is observed when the liquid droplet placed on the rough surface, has partial contact with the solid surface along with air pockets trapped underneath.

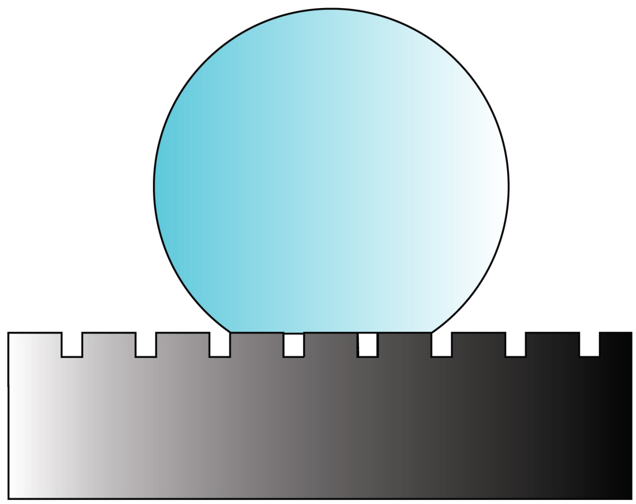

Figure 1.4: Cassie-Baxter state, the liquid droplet placed on the surface, has partial contact with the air and with the solid surface.

Using the Cassie-Baxter model, the apparent contact angle can be calculated on a rough and/or chemically heterogeneous surface as follows:

$$\cos\theta^* = f_1 \cos\theta_1 + f_2 \cos\theta_2 \tag{1.3}$$

where f_1 and f_2 are the fractional areas for which the apparent contact angle are θ_1 and θ_2, and with $f_1 + f_2 = 1$ for unity. The contact angle of a droplet on a rough surface is then dependent on the contact angle with air (180°) and solid surface θ_E. Thus, we can define the equation with θ_{Eq} being the contact's angle of on the flat surface, Φ_S being the solid fraction underneath the droplet, and with θ^* to be the apparent contact angle on the rough surface:

$$\cos\theta^* = \Phi_S(1 + \cos\theta_{Eq}) - 1 \tag{1.4}$$

with Φ_S to be the ratio of the contact area underneath the liquid to the projected area and can be obtained as shown below:

$$\phi_S = \frac{b^2}{(a+b)^2} \tag{1.5}$$

and consequently, the apparent contact angle from the Cassie-Baxter state results in a larger contact angle for hydrophobic surfaces with $\theta_{Eq} > 90°$. Liquid droplets do not have the same contact angle compared to Young's angle in Wenzel and Cassie-Baxter models. Though, in Cassie-Baxter's state, the contact angle hysteresis is lower as a result of the air trapping and small solid fraction than that of the droplet contacts when compared with the Wenzel state. In addition, for liquids with low surface tension, in the Cassie-Baxter state, the contact angle can be larger than 150°. Hence, the Cassie-Baxter state is favored in the design of superhydrophobic, superoleophobic, or superomniphobic surfaces.

1.4 Transportation of Droplets on Textured Ratchet Tracks

Solid-liquid area fraction can be used to create a surface energy gradient as first shown by Shastry et al. where the droplets on the surface move to a larger contact area to reduce their surface energy. With the help of a speaker, that applies vertical vibrations, lets the drops overcome the contact angle hysteresis [29]. In the following study, Duncombe et al. illustrated another design to achieve long-range transportation of droplets, and this was called textured ratchet tracks [30]. This was composed of periodically arced shaped pillar arrays [42]. A schematic of this design is shown in Figure 1.5, where the back and leading-edge contacts areas are different on the ratchet track.

The leading edge of the droplet is aligned with the arc, while the back edge curves in the opposite direction. In consequence, the leading edge has a larger contact area than that of the back edge which pins the droplet to the front edge 1.6. Applying the vertical vibration to match the threshold frequency and acceleration, the contact line starts its oscillation. After each cycle, the contact

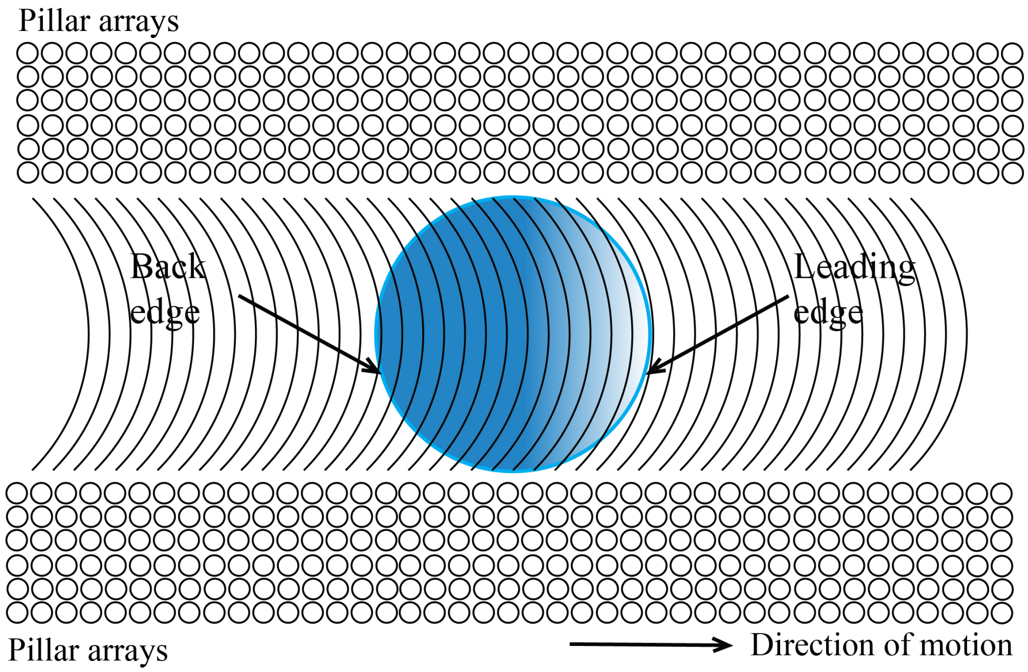

Figure 1.5: The schematics of the liquid droplet on the textured ratchet track

line is observed to expand and contract. As the stage starts moving, the edges begin to move outwards and the droplet starts wetting (advancing) and dewetting (receding) when then the edges moving inwards. Tis oscillation is at its strongest amplitude at the resonance frequency[43]. In result of the contact angle hysteresis, the contact line remains pinned for small agitation amplitudes. The drop starts advancing and receding during each oscillation period as the contact line is de-pinning for a threshold amplitude. The oscillation, as noted, is symmetric for an isotropic horizontal surface. The motion does not agitate the drop's center of mass and does not move it in the horizontal direction. Along its leading edge, the semi-circular rungs are able to provide pinning of the drop footprint continuously, though only intermittently along its trailing edge. Hence, the dewetting angle (receding) at the leading edge is small compared to the trailing edge ($\theta_{LR} < \theta_{TR}$), as well as the wetting angle (advancing) is larger at the leading edge than at the trailing edge ($\theta_{LA} > \theta_{TA}$). In consequence of the difference between receding contact angles being larger than of the advancing contact angle, the drop will a)

b)

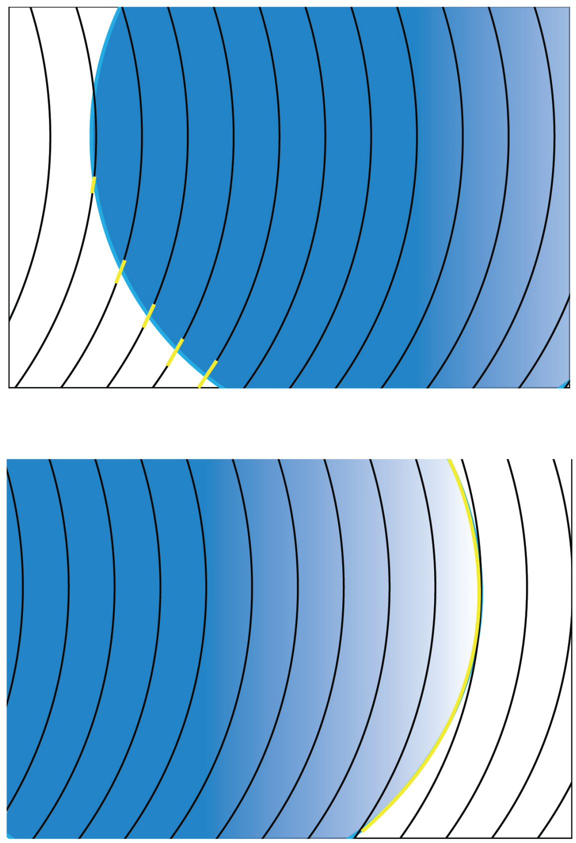

Figure 1.6: (a) The back edge asymmetry of the droplet in the opposite direction with the track arc curvature, (b) The front edge of the droplet in parallel with the track arc curvature

experience a net force forward while dewetting and a net force backward while wetting, and its sum does not add up to zero. In order to propel a drop, which has V as volume, it is needed to vibrate the system around its resonance frequency f_V. The velocity of the drop can be determined by $v = nsf_V$, with n denoting the number of ratchet rungs over which the drop passes in one oscillation, s denoting the rung spacing, and the resonance frequency f_V. As we define γ to be the surface tension of the liquid, it can be then deduced that v and f_v proportional to $\sqrt{\frac{\gamma}{V}}$. n, as shown by Duncombe et al., can be derived from the time-varying lateral force along the contact line in motion, and the moving contact line depends on design parameters such as curvature, width, and spacing of rungs plus the intrinsic contact angle of their surface material [43].

1.5 Controlling Liquid Droplets with Texture Ratchets

A surface with asymmetric features on the microstructure level, which can propel drops when vibrated can be defined as a texture ratchet. In order to control the motion of drops with different sizes, threshold frequencies need to be determined as resonance frequencies are dependent on drop volumes [43]. Design parameters such as microscale geometry and surface wettability, operation parameters such as drop volume and viscosity, vibration frequency and amplitude, and performance parameters such as droplet velocity, are necessary to help us determine the physical mechanism behind the droplet transport. To move the liquid droplets, texture ratchet can be used as an attractive low-cost platform for lab-on-a-chip applications [43]. Textured ratchets provide an asymmetric pinning force along the three-phase contact line of a droplet and as a result, when it is imposed by vertical vibration, it overcomes hysteresis and beings motion. At the resonance frequency of the droplet, the vibration amplitude of the substrate needed is at the lowest value. The resonance frequency is dependent on the droplet volume and viscosity [43]. Moreover, it is demonstrated that droplets can be addressed by their volume and viscosity, which enables us to distinguish between them when they are present on the same surface. Ratchets are well-studied for generating motion. In the recent application of the ratchets, Alvaro et al. and Jihua et al. have employed saw-tooth geometries [44, 45] and Lagubeau et al. and Shukri et al. have used vibrations [46, 47] or anisotropic nanostructures like Malvadkar et al. and Koray et al. have employed [24, 48] to induce asymmetry for liquid transport.

In this study, an automated image processing software was used to record drop position and contact angles as a function of time. As observed the stage vibration has caused the drop to have cyclic oscillations which result in expansion

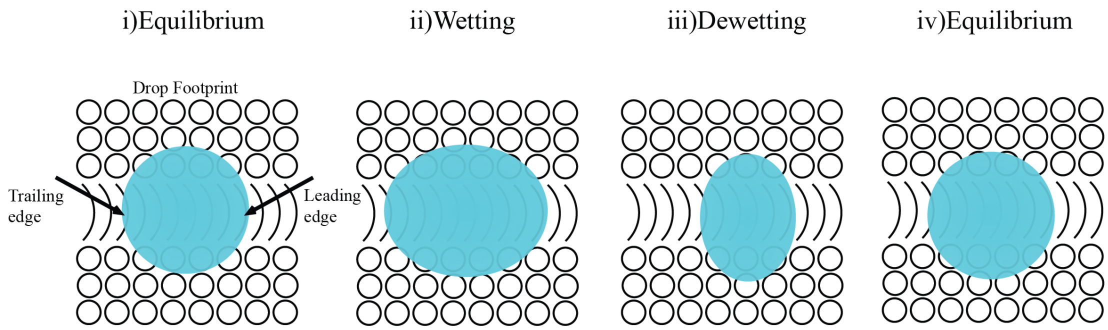

Figure 1.7: The alternate motion of the droplet: advancing (wetting) and receding (dewetting) is set in motion when we impose vertical sinusoidal vibration on the track.

and recession of the drop footprint.

1.6 Modeling

Developing a model for droplet motion on ratchet surfaces is essential to understand the dynamics, and it has started gaining more importance in recent years [49, 22, 18]. The major challenge of such a task is the non-linearity of droplet motion [47, 50, 51]. A great example of modeling attempts is done by Y. Dong's system. In their work, Y. Dong presents an interesting representation of a motion similar to the droplet motion. The suggested system captures important features such as leading and tailing angles. Moreover, the (3 masses , 3 springs) system creates a pattern of motion that can be compared to that of the droplet as seen in Figure .

The compact model presenting the droplet as a three-mass system, which consists of the leading edge, trailing edge, and body. Its aim is to simplify the vertical vibration applied to the ARC (anisotropic ratchet conveyors) pattern which propels a lateral droplet motion on substrates, horizontal or inclined. In Dong's work [52], they have introduced a model of a damped harmonic oscillator that

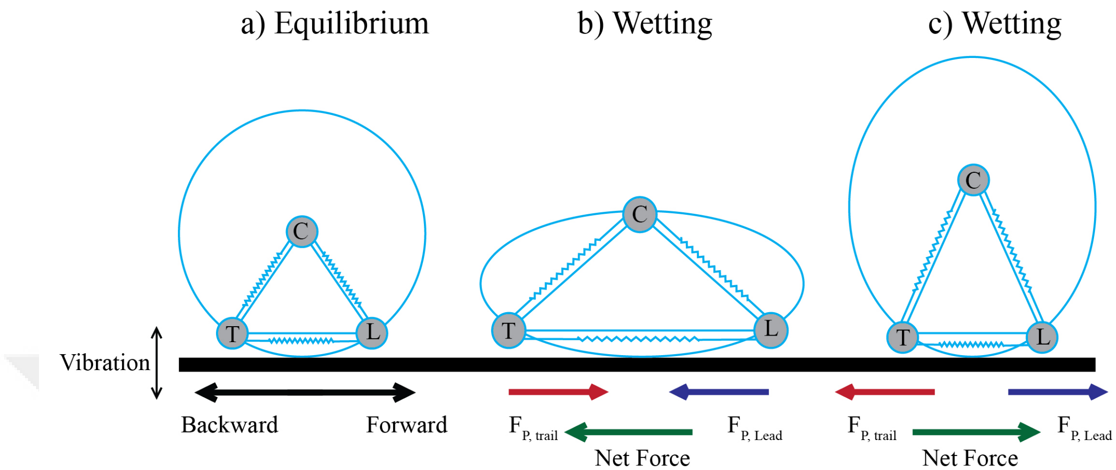

Figure 1.8: Theoretical model of droplets on ARC devices

is able to capture the key features of a moving droplet on a ratchet. The simulation has shown a good level of resemblance with the experimental data. The non-dimensionalization was utilized to show the similarity between the behavior of droplet vibration on ARC devices, and that of a harmonic oscillator-based system. Though, in this non-dimensionalization, the viscous damping was not taken into consideration when the resonance frequency was being observed. It can only be considered to be accurate to describe the droplet behavior before the lateral motion occurs. However, as noted in [52], damping effects are to be considered when the droplet starts to move on the track. The effects cause friction/drag inside the droplet and around its interface with the ratchet track. The damping can determine the energy dissipation, and the energy coupled into the droplet from the oscillating track. As a result of the vibration, the periodic external forces are at play on the leading and trailing edge of the droplet and are represented in the cross-sectional model as L and T respectively. They are connected to C, the center of mass, and to each other. The three masses are connected by a damped spring in the form of a triangular mass-spring-damper system. The two masses at the leading and trailing edges are m_L and m_T respectively at the contact line between the droplet and the arcs of the track, while m_C is taken to be the bulk volume of the droplet. Few assumptions are taken such as $m_T = m_L < m_C$ and the springs between T, L, and C representing the

surface tension are as follows $K_{TC} = K_{LC} < K_{LT}$. This holds only to the effect of a stiffer spring that is the pin-release events at the contact line. At rest, the springs' length is $L_{TC} = L_{LC} < L_{LT}$ and the viscous damping coefficient, given by Stokes's law as $b = 6\pi\mu R$, which is the same for all dampers. To simplify the model further, it is assumed that $F_{H,lead} = F_{H,Trail}$ and hence the net lateral droplet motion would be resulting from the asymmetric pinning forces. The difference between the lead and trail forces at the wetting face while positive for the dewetting phase [52]. This indicates that these pinning forces are lower during the wetting phase of the contact line and less sensitive to pinning. A simulation of this two-dimensional triangular mass-spring-damper system with friction forces and good agreement with that of the experimental data was seen, which indicates that associated parameters are to draw the characteristics and behavior of the droplet motion. The model capability arises from the main component that is the damped harmonic oscillator formulas. However, what limits its predictive capacity is that the parameters of pinning forces and liquid properties must be either determined empirically or a priory[52]. Moreover, the system proposed (3-mass-3-spring) is a linear model while the droplet motion on a ratchet track shows non-linear properties such as parametric resonance.
Therefore, the modeling of the droplet remains an unresolved problem. However, developing a concrete model can have several economical advantages. It will not only simplify droplet studies by removing the necessity of experiments but will also expand our understanding of droplet dynamics. This expanded understanding may lead to more complex applications.

1.6.1 Simulation

In the following work, a new formulation of the droplet motion is presented. The droplet-surface interaction is studied in terms of a double pendulum attached to a moving cart. The numerical model is shown in Figure-3.1. The double pendulum on a cart is a non-linear under-actuated mechanical device and is quite sensitive to any modeling error and extrinsic disturbance [53]. In Yuanhong's et al., parameters of the cart-double pendulum motion were identified by using Improved Genetic Algorithm (IGA). The task is a complex one, and especially when it is turned into a real-time situation study, as any minimal error between the model and the actual device could lead to significant adjustments. However, the usage of an accurate kinetic model proves the key to the easier transition from simulation to real-time experiment. IGA with its several parameters served to identify these physical parameters. The experimental results resembled well to that of the simulation [53]. The model in this thesis was created using MATLAB's Simscape tool which could provide us with a stable simulation of the double pendulum motion. The parameters were noted down, as well as the initial conditions. The pendulum oscillated around its center of mass for a period of time before its net movement started. The model had an anisotropic environment with an external and uniform force setting the double pendulum into motion. The equations governing its motion are a set of nonlinear, multi-variable dynamic equations which made the model exceptionally sensitive and harder to get an accurate description of our model.

1.6.2 Numerical Tools

The principal component (PCA) is a tool to further understand of the numerical results better and enhance the approach. It is used generally in the data analysis field and implemented for predictive models. The first principal component is commonly defined to be the direction maximizing the variance of the project data which was the straight line. The second component is the horizontal periodic response of the droplet as a result of the vertical oscillation of the track. Its common usage is for dimensional reduction as one is able to project data points onto the first few principal components, and hence obtaining lower-dimensional data without losing the data's variation. Another numerical tool is The Elastic Functional Data Analysis (EFDA).

It is employed to align the data with minimal loss while modeling the droplet motion as a multidimensional function making it easier for data comparison.

Then, the elastic distance between the two signals of simulation and experiment was calculated to identify the similarities. The flow of our work is as follows:

- Analyzing the images taken from the high-speed camera capturing the motion of the droplet on the textured ratchet using image processing techniques.
- The motion of the double pendulum mounted on a cart is simulated with defined parameters and initial conditions.
- The pendulum simulation results are used to recreate droplet motion numerically
- Frechet Distance is utilized to adjust the weight of the simulation to generate a better fit the experimental data
- Once the weight is optimized for the comparison between the experimental data and the simulation, the model is then chosen to re-create the motion of the droplet motion providing a theoretical framework while maintaining the key features of this motion.

The reason for choosing the inverted double pendulum as a theoretical backbone for our work is due to the fact that it is a well-studied non-linear system with matching properties such as parametric resonance and double-peak motion which makes it a good candidate for droplet modeling purposes[54, 55]. Therefore, using these tools, we developed a double-pendulum-based numerical model that provides the following advancements

- The ability to reproduce droplet motion
- Maintaining key features from the droplet motion such as the non-linear response.
- Scalability, where the model can be fine-tuned for different experimental set-up

Unlike previous works in literature, our model utilizes a full non-linear framework to represent the droplet motion. The details of the model and data processing will be presented in this thesis.

Chapter 2

Data Acquisition and Processing

2.1 Ratchet Track Design

Ratchet tracks used in the experiment were fabricated by E.Yelekli as part of their master thesis [36]. The tracks used in this study have a mushroom side profile to reduce their wettability. Tracks with different radius of curvatures (ROC) were designed and fabricated. The list of these tracks used for modeling studies is listed in the table 3.1 below.

The distance between the arc-shaped pillars and their sickness vary with each design to find the optimum dimensions. The space ratio is defined as the ratio of the pillar width to the space between two consecutive pillars. Schematic of the top view of tracks are shown in figure [?] The tracks were 0.9 mm with ROC of 1.6 mm, and 1.2 mm for ROC of 2.0 mm. ROC plays a crucial for the droplet motion and it should be enough to pin the droplet's front contact line.

Table 2.1: Ratchet Track Fabrication design

Design number	Arc width (μm)	Space ratio	Radius of curvature (μm)
1	30	1.2	900
2	30	2.0	900
3	30	2.4	900
4	50	1.2	900
5	50	1.6	900
6	65	1.2	900
7	30	1.2	1200
8	30	2.0	1200
9	30	2.4	1200
10	50	1.2	1200
11	50	1.6	1200
12	65	1.2	1200

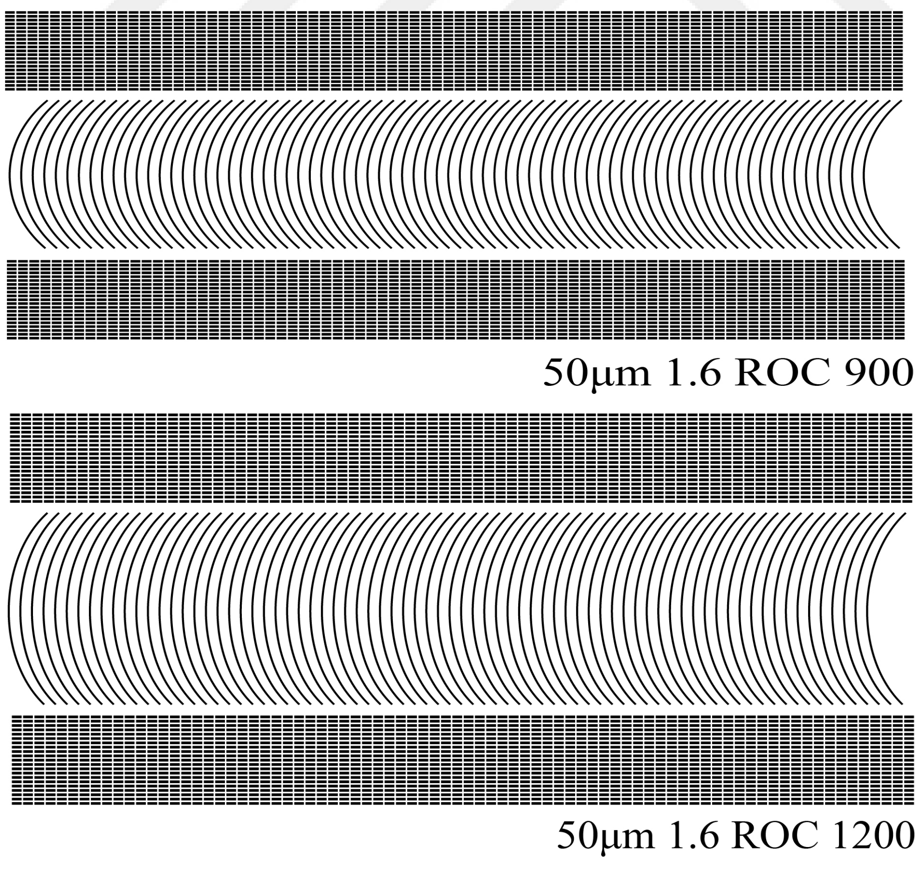

Figure 2.1: The ratchet with 50 μm arc width, 1.6 space ratio and 0.9mm (900 μm) ROC, the ratchet with 50 μm arc width, 1.6 space ratio and 1.2 mm (1200 μm) ROC

To create a superhydrophobic area to prevent droplets from falling out of the track, pillar arrays were put to both sides of the tracks.

2.2 Experimental Set-up

The experimental sety-up for obtaining data of droplet motion is composed of a function generator (GW Instek-type SFG 2004), a power amplifier (Bruel Kjaer-type 2718), a vibration exciter (Bruel Kjaer Type 4809), an accelerometer, an oscilloscope (DSO-X2012A), a high-speed camera (Phantom) and a high-intensity light source, as shown in Figure 2.2.

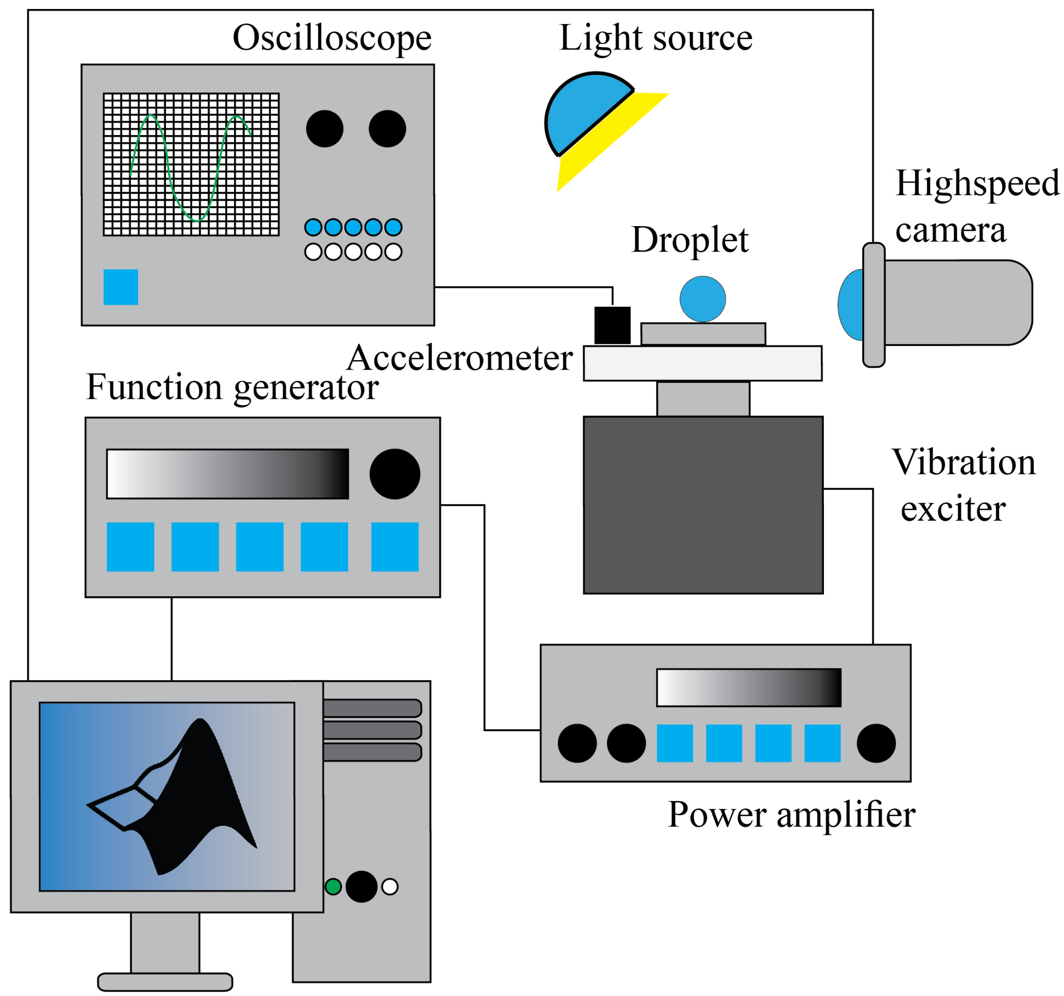

Figure 2.2: A schematics of the experimental setup

The power amplifier intensifies the signal produced by the function generator and then transmits it to the vibration exciter. As the track starts its vertical vibrations, the contact line of the droplet beings to oscillate, and once the threshold amplitude is reached, it starts propagating. In order to measure the acceleration, an accelerometer is placed on the exciter platform and the frequency value is specified through the function generator. The droplet movement is recorded with the high-speed camera and then the image data were processed to characterize the droplet motion. The schematics of the setup is shown in Figure 2.2

2.3 Image Processing

The data comes in the form of images recorded by using the high speed camera as shown in Figure.2.4.

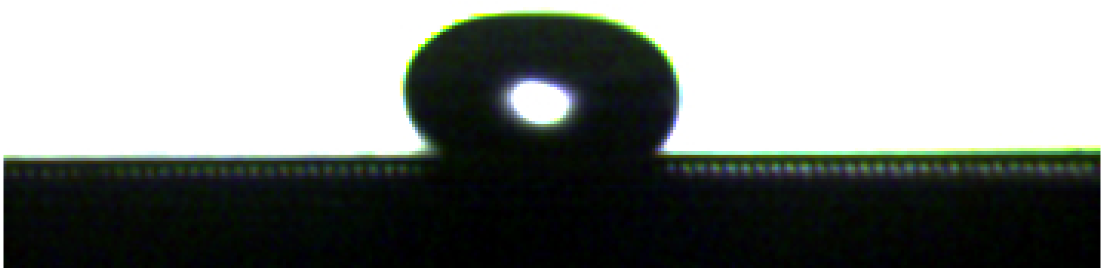

Figure 2.3: Example of an input image

Matlab's Image-processing toolbox has been used to make measurements on the input images. Traditional image processing techniques have been utilized to pre-process the images in RGB color format. Functions such as *Imbinarize*, *rgb2gray*, and *imclose* are used to create and binarize 2-D grayscale images, while *imopen* perform morphological opening. The opening operation first erodes the image, then dilates the eroded image using an identical structuring element for both operations. This is particularly a preferred approach if the objects of interest are relatively larger than undesired objects in the image. This method removes small objects while preserving the shape and size of larger objects. The results are shown in Figure.2.4

The edges within the images are detected using Matlab's Canny edge detection algorithm. Once the edges are detected, the straight line representing the track is found using Hough transforms as shown in Figure.2.5.

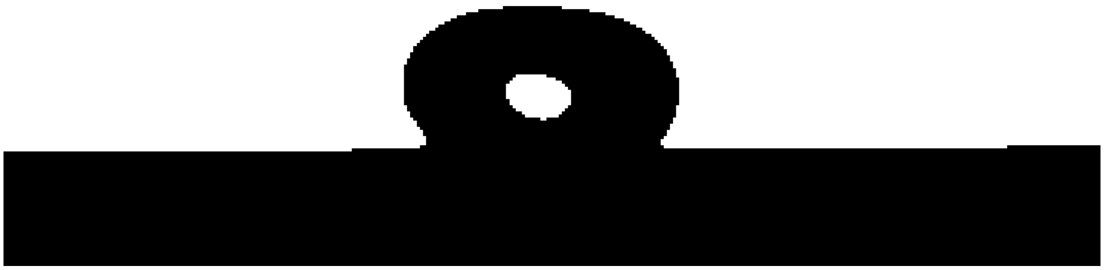

Figure 2.4: Resultant image after pre-processing.

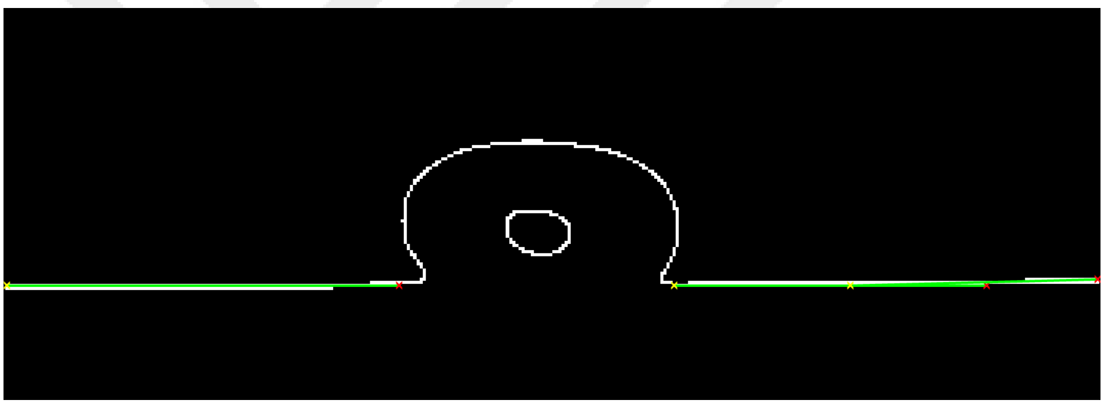

Figure 2.5: In white, the edges are detected using Canny edge detection method. In yellow, straight lines represent the edge of the track.

The track is assumed to be completely horizontal. Hence, the level of the track can be approximated according to Equation.2.1. Once the stage level is detected, the pixels on or below the stage are removed leaving only the droplet edges in the frame. The longest edge represents the outer boundary of the droplet which is the edge of interest as shown in Figure.2.6

$$Y = \frac{\sum_{i=1}^{N} y_i}{N} + \epsilon \tag{2.1}$$

Where: Y = approximated level of stage,

$y_i = y$ components of data points detected on the lines

N = total number of pixels detected on the line

ϵ = small number of pixels added to account for errors

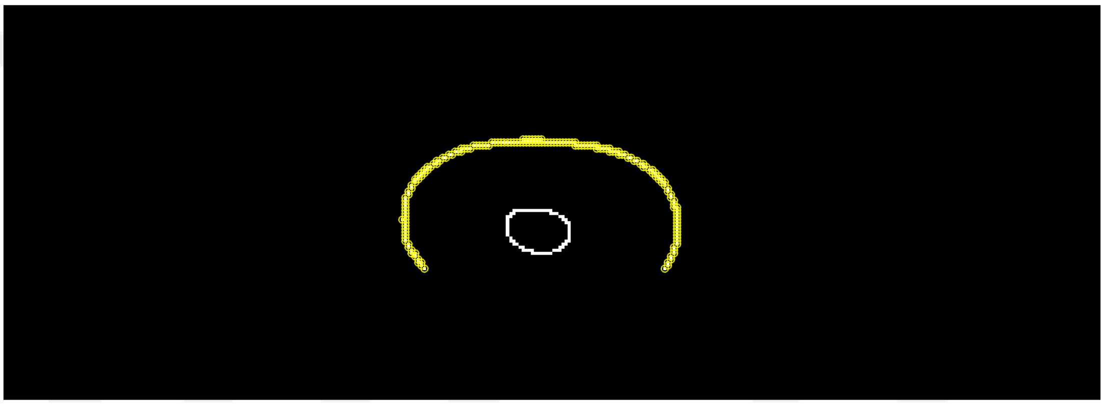

Figure 2.6: Only droplet edges are kept after stage and background are removed. The edge of interest of highlighted in yellow.

The segmented edge contains three key data points:

- X_0 : x location of the top of the droplet
- $X_{leading}$: x location of the leading edge of the droplet
- $X_{trailing}$: x location of the trailing edge of the droplet

These data points are calculated according to the following:

$$X_0 = X|_{y=max(Y)} \tag{2.2}$$

$$X_{leading} = X|_{y=min(Y^*)} \text{ where } Y^* = Y(x > X_0) \tag{2.3}$$

$$X_{trailing} = X|_{y=min(Y^{**})} \text{ where } Y^{**} = Y(x < X_0) \tag{2.4}$$

The data points shown in Figure.2.7 are continuously tracked throughout the experiment and used to create the droplet model.

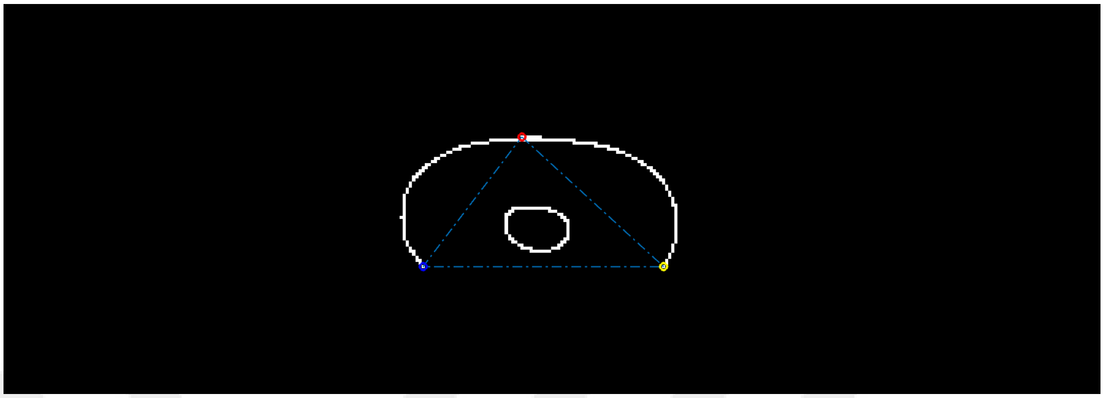

Figure 2.7: The three important data points: X_0 in red, $X_{leading}$ in blue, and $X_{trailing}$ in yellow.

2.4 Experimental Observations

The motion of a water droplet ($8\mu l$) on the ratchet track with arc width 50 μm (1.6) is shown in Figure 2.8. At 63 Hz, and 4 g the droplet started to move at the minimum acceleration value, also known as the threshold value of acceleration. The images were taken at different intervals to illustrate the droplet behavior during its motion on the ratchet track. The shape of the droplet as explained in Shastry work[29] is changed due to the alternating wetting and dewetting behavior of the droplet and it continues to change under the effect of the vertical vibration. The contact line oscillates and as a result of the asymmetry of the design, it turns into a net movement, and to analyze the motion of water transportation, the video is processed.

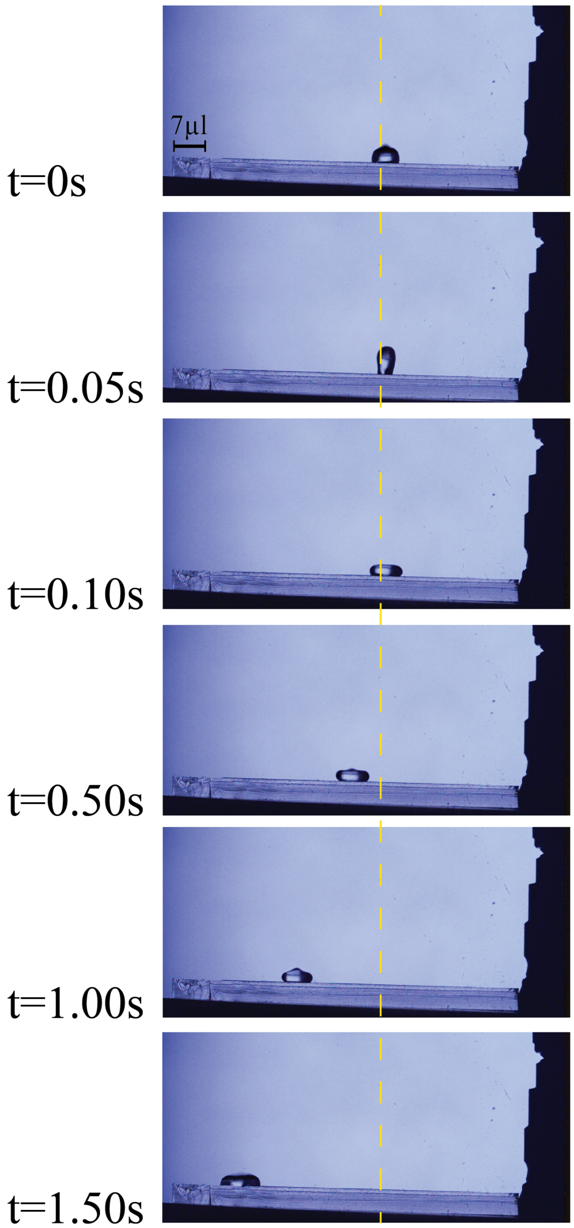

Figure 2.8: Images of water droplet (7 μl) transported on the ratchet track of 50 μm (1.6) taken by the high-speed camera. Transportation is at 65 Hz and 9 g.

The frequency and threshold value of acceleration were tried for different volumes, tracks, and frequencies to calculate the average velocity for droplets in Yelekli's paper [36] of 50 μm (1.6), 50 μm (1.2), and 65 μm (1.2). The frequency and acceleration of the droplet depend on the viscosity and volume of the droplet[29].

Chapter 3

Droplet Modeling

A great amount of experimental work has been dedicated to understand the experimental properties and dynamics of droplet motion on textured ratchet tracks [52, 56]. However, the efforts for modeling the droplet motion have been less extensive. This is due to the complex and non-linear nature of this motion [57]. Some work has shown a potential modeling approach [52]. Dong's et al. model the droplet-ratchet surface interaction as a 3 mass, and 3 spring system [52]. Dong's et al. could demonstrate that nondimensionalization shows consistent behavior for droplets of different volumes. Their model captures essential features of horizontal droplet motion that is due to the surface asymmetry arising from the vertical vibration. Such models are able to reproduce important features of the droplet motion [52]; however, they are linear models whereas the droplet motion is non-linear. The model proposed in this thesis is based on the results of a double pendulum motion simulation. Based on the experimental observations and from several simulations it can be seen that both the double pendulum and droplet motion show resembling responses. Moreover, the double pendulum is a well-studied parametric resonator system [58, 59] making it an ideal candidate for droplet motion modeling. The pendulum simulation set-up is shown in Figure 3.1.

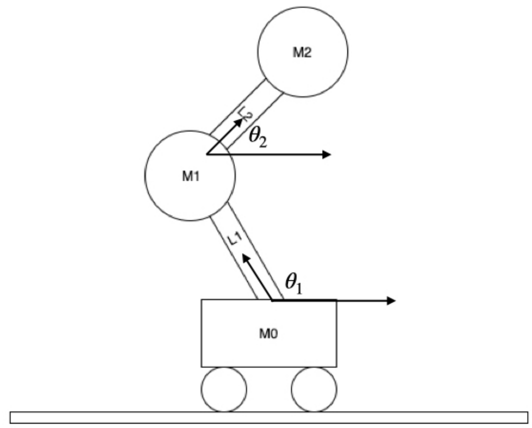

Figure 3.1: Schematic showing the double pendulum attached to a moving cart on a track.

3.1 Double Pendulum Model

The theoretical backbone of this model is a double pendulum attached to a moving cart, as shown in Figure 3.1. The cart is assumed to be a mass-less object sliding with no friction on the track that resides on. For simplicity, the model can be assumed to be two rods connected with a joint that allows friction-less motion and mounted on top of a mass-less cart. The simplified representation of the model is shown in Figure 3.2.

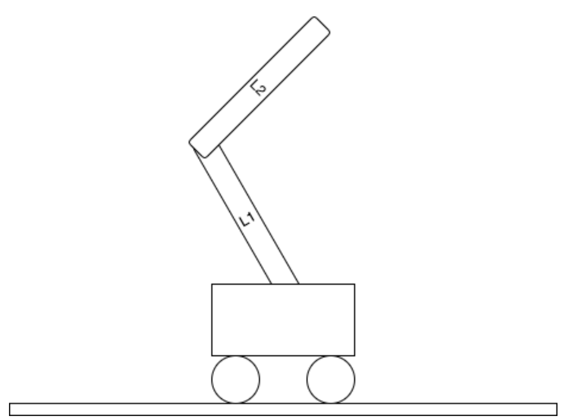

Figure 3.2: Schematics showing a simplified representation of a moving inverted double pendulum

3.2 Proposed Model

A double pendulum is comparably easier to study as it represents a non-linear model that can be employed to recreate the behavior of the droplet on the ratchet track [60]. The non-linear motion of the double pendulum on a cart has been well investigated [61, 62]. As seen in Figure 3.2, the model is built of two masses on a double pendulum attached to a moving cart on a horizontal track. The surface on which the cart moves is frictionless, and the cart and pendulum are considered to be mass-less objects. The model has been recreated using MATLAB's Simscape tool to produce a stable simulation of the double pendulum motion as shown in Figure 3.3.

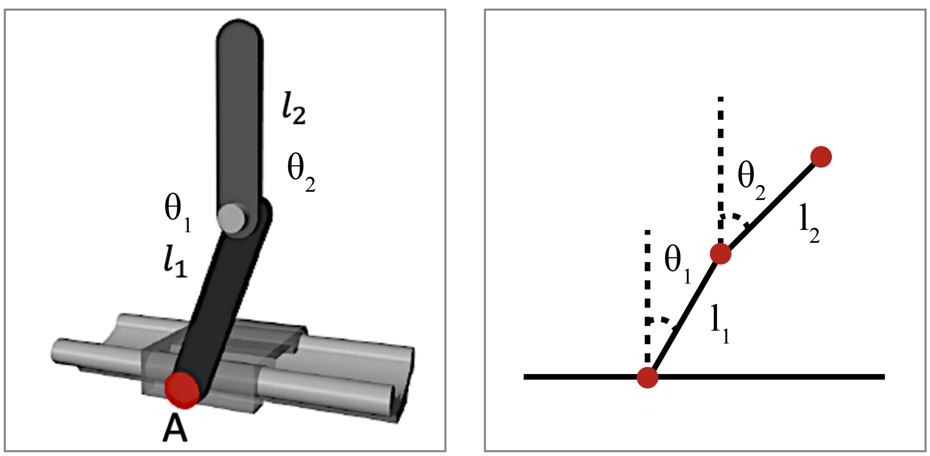

Figure 3.3: A sample behavior of an inverted double pendulum on a sliding cart obtained using Simscape Multibody in MATLAB. The visual presentation of the simulated system. The double pendulum dimensions are as follows $L_1 = 18cm$, $L_2 = 14cm$, with a uniform density of $2700kg/m^3$. The initial angles are $\theta_1 = 0$ and $\theta_2 = -20°$. The double pendulum is set not to have any initial velocity.

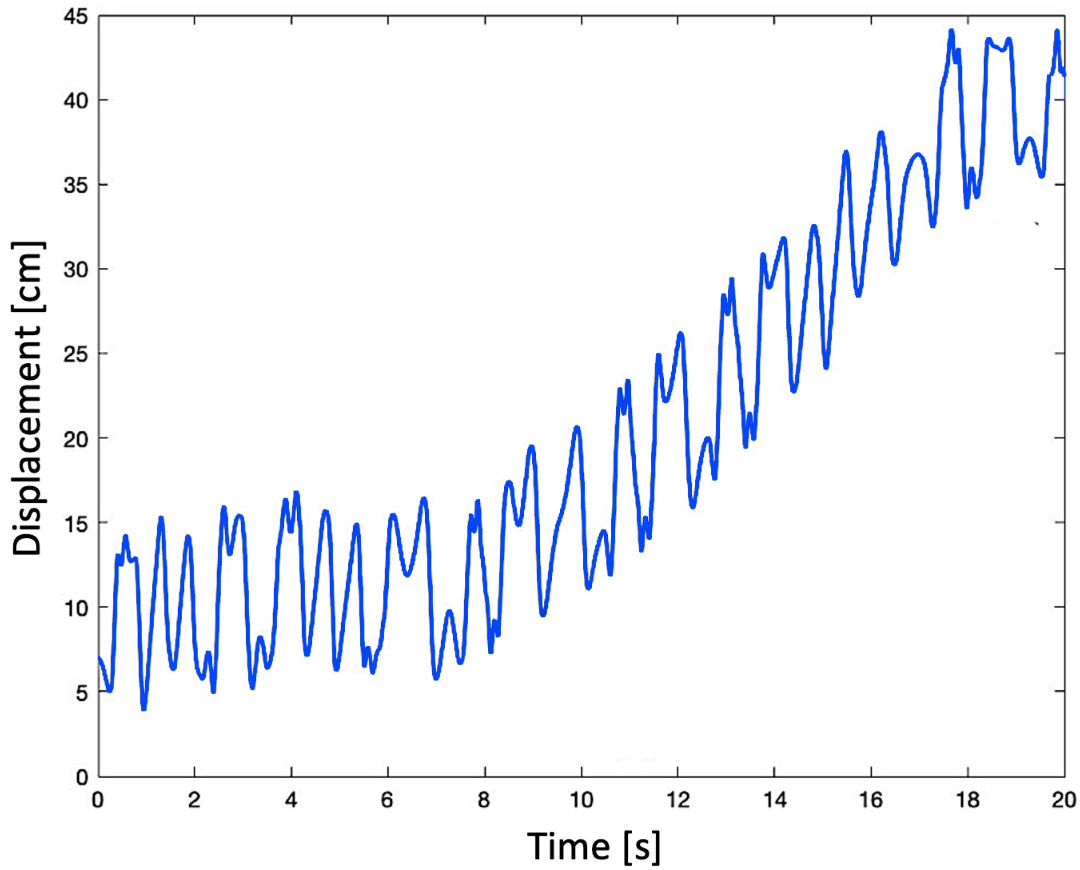

Figure 3.4: Displacement of the pendulum from point A with respect to time under the effect of an external bias force is applied.

In the figure 3.3, these parameters and initial conditions are shown. The simulation of the model exhibits two phases of motion similar to that of the droplet motion. The pendulum, under an external bias, starts to oscillate around its center of mass for a certain amount of time before the net movement is forward as shown in Figure 3.4. The environment in which it is modeled is anisotropic where the force setting the double pendulum into motion is uniform and external. The model is constrained by a set of nonlinear, multi-variable dynamic equations given in Equation 3.1. The latter makes it a volatile model and hence exceptionally sensitive to errors. Thus, the parameters were calibrated and initial conditions were chosen precisely[63] to avoid the errors.

$$\begin{aligned} &a\,\ddot{x} + b\,\cos\theta_1\ddot{\theta}_1 + c\,\cos\theta_2\,\ddot{\theta}_2 - b\,\sin\theta_1\,\dot{\theta}_1^2 - c\,\sin\theta_2\,\dot{\theta}_2^2 = F\,,\\ &b\,\cos\theta_1\,\ddot{x} + d\,\ddot{\theta}_1 + e\,\cos\theta_{21}\,\ddot{\theta}_2 - e\,\sin\theta_{21}\,\ddot{\theta}_2^2 - b\,g\,\sin\theta_1 = 0\,,\\ &c\,\cos\theta_2\,\ddot{x} + e\,\cos\theta_{21}\,\ddot{\theta}_1 + f\,\ddot{\theta}_2 + e\,\ddot{\theta}_1^2\,\sin\theta_{21} - c\,g\,\sin\theta_2 = 0\,,\end{aligned} \tag{3.1}$$

where $\theta_{21} = \theta_2 - \theta_1$ and

$$\begin{aligned} a &= m_0 + m_1 + m_2\,, & b &= \tfrac{1}{2}m_1L_1 + m_2L_1\,, & c &= \tfrac{1}{2}m_2L_2\,,\\ d &= I_1 + \tfrac{1}{4}m_1L_1^2 + m_2L_1^2\,, & e &= \tfrac{1}{2}m_2L_1L_2\,, & f &= I_2 + m_2L_2^2\,. \end{aligned}$$

with m_0 being the mass of the cart, m_1, m_2 the masses of the lower and upper pendulum arms respectively, L_1, L_2 the length of these arms, and x the position of the cart as a monitored output of the simulation.

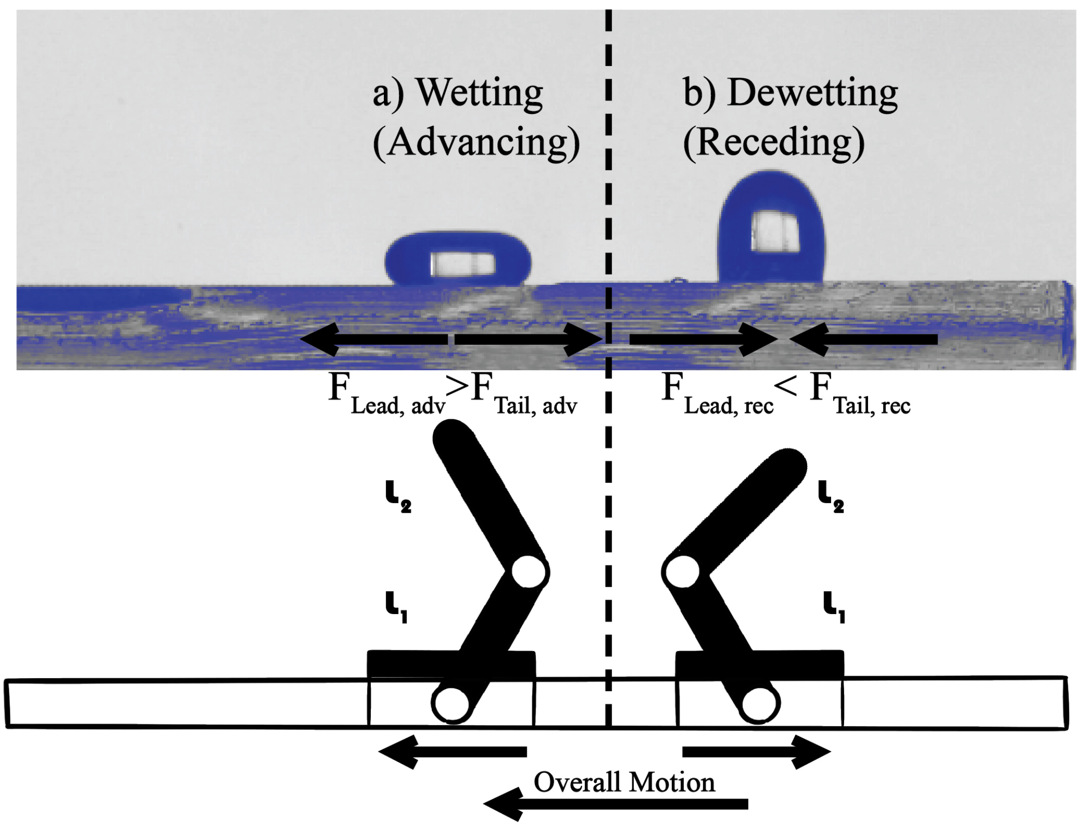

Figure 3.5: The droplet and pendulum system in altering states.

Figure 3.5 shows the corresponding pendulum model with respect to the droplet moving on the surface. In a) wetting state: the droplet is in the advancing stage, it undergoes less resistance in the direction of the motion, and as a result of the track's texture. Below is the pendulum similarly sliding in the direction of the bias. In b) dewetting state: The droplet is in the receding stage, its leading edge of the droplet resists the displacement whereas the tail edge moves in the direction of the motion. Similarly, the pendulum, moving in the opposite direction of the motion, encounters resistance by adding the bias force to the numerical model.

Two apparent motion modes that the droplet undergoes on the ratchet track can be observed in the motion of the pendulum on the track 3.5. The two modes of the pendulum on a cart resemble the wetting and dewetting state of the droplet motion (Figure 3.5). The pattern of the droplet motion can also be observed in the overall motion of the pendulum (Figure 3.4). The droplet will oscillate around the center of the contact line before overcoming hysteresis. Though, before advancing, the pendulum will oscillate around its center of mass which also exhibits similarity to the droplet motion on the ratchet track.

The data collected from the experiment and the simulation ran operate in different spaces, meaning different frequency domains, time, and space scales (Figure 3.6). Thus, the dimensions of the two systems are to be normalized to have a relevant comparison between the two data. In this study, the only focus will be on the pattern the droplet generates moving on a ratchet track. The two systems show similar features as shown in Figure 3.6.

The Elastic Functional Data Analysis (EFDA) has been employed to quantify the comparison of the two data. EFDA allows data alignment with minimal loss as it models the droplet motion as a multidimensional function. Using this alignment, the elastic distance between the two signals is calculated and help identifying the similarity between the model and the experimental data.

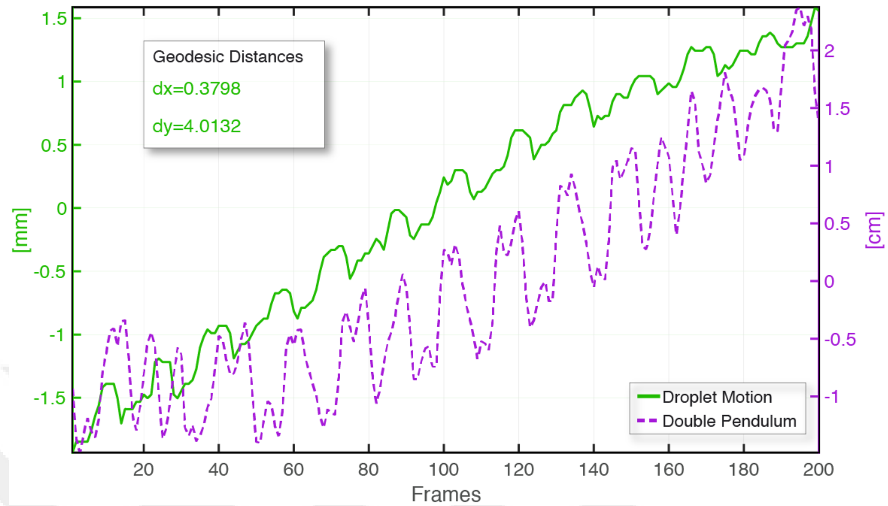

Figure 3.6: In green, the motion of a water droplet on an oscillating track with a frequency of 60 Hz is shown. In purple, the actuated double pendulum's motion of dimensions $L_1 = 18cm$, $L_2 = 14cm$, uniform density of $2700kg/m^3$, initial angles of $\theta_1 = 0$ and $\theta_2 = -20°$. Both of the functions were normalized and the elastic geodesic distance is then calculated (dy: amplitude distance, dx: phase distance).

3.3 Methodology

After examining the experimental data, it can be said that the droplet motion is composed of two major components: oscillating signal and driving signal. The latter is supported with PCA (Principal Components Analysis), in which the first two principle components recover 84% of the information as Table 3.1 shows.

Table 3.1: Experimental data PCA. 84% of the data could be explained by the first two Principle Components (PC)

Principal component	1st	2nd	3rd	others
Variance	75.85	8.49	6.04	9.62
Cumulative variance	75.85	84.34	90.38	100

The first component, the straight line, can serve as the driving force setting the droplet into forward motion. The second component encloses the horizontal

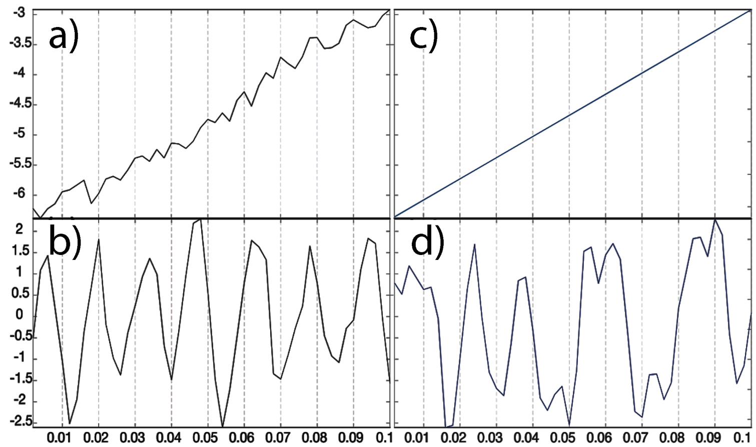

Figure 3.7: a) First PC, b) second PC, c) first component of the model, d) second component of the model

periodic response of the droplet undergoing the vertical oscillation of the track. Adding this observation to the numerical solution of the double pendulum on a cart will form the basis of the modeling approach followed. Equation 3.2 characterizes the model of the system, with S being the normalized signal of the double pendulum oscillation before its propagation, V being the velocity of the droplet motion, ϕ being the phase difference, and α being the parameter controlling the non-linearity of this model. In more details, Equation 3.2 overlays the driving signal, $Vt+\phi$, and the pendulum oscillations (shown in Figure 3.7 c,d) following α as αS, and $Vt+\phi$ as parameters. The result of the model is $F(t)$ 3.2.

$$F(t) = Vt + \phi + \alpha S \tag{3.2}$$

An intrinsic parameter tailoring the model to the experiment is configured by α. α can be used to maximize the similarity exhibited between the model and the experiment using Fréchet distance[64], given in Equation 3.3.

$$Fr(f,g) := \inf_{\alpha,\beta} \max_{t\in[1,2]} d(f(\alpha(t), g(\beta(t))) \tag{3.3}$$

with $d(f,g)$ being the Euclidean distance between f and g, the latter are taken in terms of α and β.

Various weights for (α) were used creating different models. The distance between that created model and the experiment is the optimization factor controlling the processing analysis flow chart as shown in Figure 3.8.

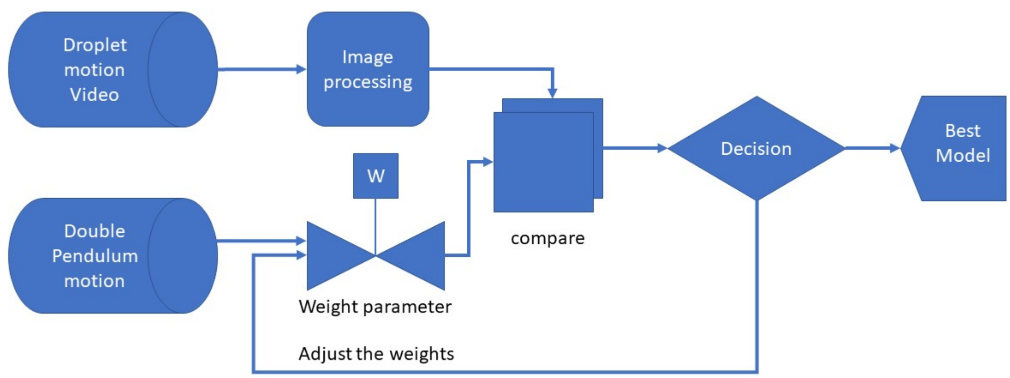

Figure 3.8: Flow chart explaining the modeling, and algorithm. The weight parameter α is varied in according to the elastic distance.

3.4 Results and Discussion

Employing the pipeline proposed in Figure 3.8, the parameters are varied in Equation 3.2 in order to minimize the distance between the experimental results and the output of the model. The signal was successfully recreated resembling the droplet motion by minimizing the Fréchet distance, after showing the resemblance between the droplet motion and the moving double pendulum.

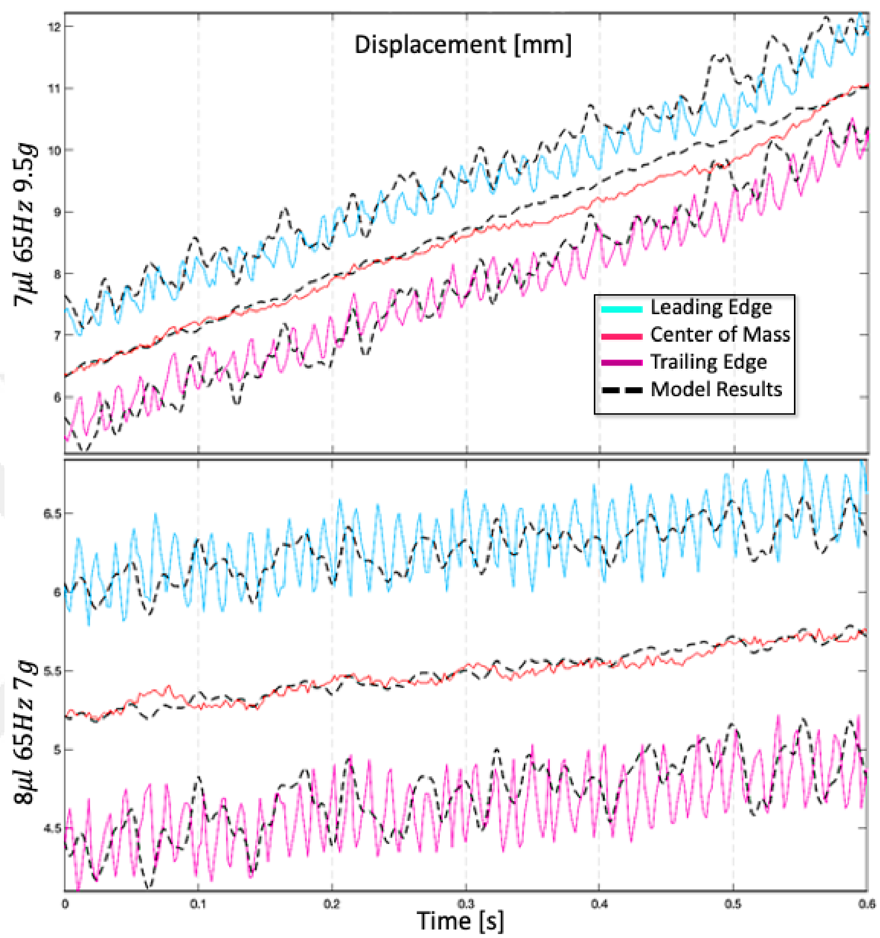

Figure 3.9: Comparison of results obtained by the pendulum model with the experimental data of droplets acquired for different volume and actuation parameters.

To verify the proposed method, it was tested for different experimental data. Part of the results is shown in Figure 3.9. The model is able to capture the pattern behavior of the droplet motion and can reproduce different approximations for leading and receding edges while preserving the difference between and amplitudes between the two edges. This simple model, as presented in Figure 3.9, is able to construct the double peak effect usually observed in the droplet motion. Nevertheless, the obtained experimental data does not hold this effect as a feature. It fails to adjust to the input. Therefore, it can be pointed out that there is a necessity to develop a far more complex system in order to reproduce every possible experimental output. Nevertheless, the simple superposition between a linear equation and a double pendulum simulation can be used to recreate the general motion of a droplet while keeping its double peak feature.

Chapter 4

Conclusion and Future work

In this work, a different approach is proposed to understand the motion of droplets on a ratchet textured surface, which are composed of pillar arrays as described in chapter 2. The pillar arrays compose a texture on the surface than creates an energy gradient. As discussed, this gradient sets the droplet into a directional propagation once the track is set into oscillation. The oscillations expand and contract the droplet footprint on the track, leading to an overall motion.

The main purpose of this work is to provide a model that can capture this interaction. The theoretical backbone of our work is a double pendulum mounted on a cart. The data was deducted from the experimental data and from several numerical observations, in which the resemblance between the double pendulum and the droplet motion has been observed. This similarity between the two systems makes the double pendulum a good choice for our modeling purposes. The double pendulum system is thoroughly studied as a nonlinear system [58, 59] and it sets the basis for the droplet motion. The method, used to highlight the similarity between the double pendulum and droplet motion, is the elastic functional data analysis explored in chapter 3. By using elastic functional data analysis, the signals generated by droplet motion and by pendulum motion are overlapped which allows a qualitative comparison. This comparison is showed in chapter 3, where the two system shows great qualitative similarities.

Moreover, a numerical model of a double pendulum was proposed. The model is constructed based on the results of principal component analysis of the experimental data. Then it is quantitatively compared to the experimental data using Fréchet distance, for similarity observations. The Fréchet distance is used for parameter turning in order to get the best fitting results generated from the proposed model.

The key features in common between droplet motion and double pendulum motion are a double peak pattern and the hysteresis before setting into motion, and their parametric behaviour. The two systems, the double pendulum on a cart and droplet motion, are highly non-linear complex systems with no analytic solution. Advanced models, however, were investigated to describe the complex behavior of the double pendulums. Hence, several techniques were employed to unravel the characteristics of the droplet motion, which can lead to droplet-based advanced applications in the near future.

The theoretical approach can benefit from existing studies instead of starting from the preliminary stages. We hope further studies can explore the possibility of utilizing the double pendulum for a more thorough numerical model. A modification on the double pendulum equations of motion can lead to interesting results. Moreover, a parameters mapping between the two systems can expand our understanding of droplet motions. Therefore, by following a more analytical approach, and by studying the non-linear model of the double pendulum through various computational methods, the loss generated by small errors can eradicate, different initial conditions can be explored in depth. To further enhance the study, it is recommended to investigate the similarity between the two systems presented using different computational and mathematical tools.

Hence, in this study, it can be seen that a double pendulum mounted on cart can be qualitatively and quantitatively compared to double pendulum. Moreover, this work could be considered as an initial droplet motion modeling effort based on non-linear systems such as double pendulum.

Bibliography

[1] Y.-D. Ma, K. Luo, W.-H. Chang, and G.-B. Lee, "A microfluidic chip capable of generating and trapping emulsion droplets for digital loop-mediated isothermal amplification analysis," *Lab Chip*, vol. 18, pp. 296–303, 2018.

[2] A. M. Nightingale, S.-u. Hassan, G. W. H. Evans, S. M. Coleman, and X. Niu, "Nitrate measurement in droplet flow: gas-mediated crosstalk and correction," *Lab Chip*, vol. 18, pp. 1903–1913, 2018.

[3] I. Lignos, V. Morad, Y. Shynkarenko, R. M. Bernasconi, Caterina nad Maceiczyk, L. Protesescu, F. Bertolotti, S. Kumar, S. T. Ochsenbein, N. Masciocchi, A. Guagliardi, C.-J. Shih, M. Bodnarchuk, A. J. deMello, and M. V. Kovalenko, "Exploration of near-infrared-emissive colloidal multinary lead halide perovskite nanocrystals using an automated microfluidic platform," *ACS Nano*, vol. 12, pp. 5504–5517, 2018.

[4] H. Feng, T. Zheng, M. Li, J. Wu, H. Ji, J. Zhang, W. Zhao, and J. Guo, "Droplet-based microfluidics systems in biomedical applications," *Electrophoresis*, vol. 40, pp. 1580–1590, 2019.

[5] X. Lin, X. Huang, K. Urmann, X. Xie, and M. R. Hoffmann, "Digital loop-mediated isothermal amplification on a commercial membrane," *ACS Sensors*, vol. 4, pp. 242–249, 2019.

[6] C. S. Karamitros, M. Morvan, A. Vigne, J. Lin, P. Gruner, T. Beneyton, J. Vrignon, and J.-C. Baret, "Bacterial expression systems for enzymatic activity in droplet-based microfluidics," *Anal. Chem.*, vol. 92, pp. 4908–4916, 2020.

[7] G. Mahmud, C. J. Campbell, K. J. M. Bishop, Y. A. Komarova, O. Chaga, S. Soh, S. Huda, K. Kandere-Grzybowska, and B. A. Grzybowski, "Directing cell motions on micropatterned ratchets," *Nature Physics*, vol. 5, no. 8, p. 606–612, 2009.

[8] N.-T. Nguyen, S. T. Wereley, and S. A. M. Shaegh, *Fundamentals and applications of microfluidics.* Artech house, 2019.

[9] L. Shang, Y. Cheng, and Y. Zhao, "Emerging droplet microfluidics," *Chem. Rev.*, vol. 117, no. 12, pp. 7964–8040, 2017.

[10] S. Sohrabi, N. Kassir, and M. K. Moraveji, "Droplet microfluidics: fundamentals and its advanced applications," *RSC Advances*, vol. 10, p. 27560, 2020.

[11] S.-Y. Teh, R. Lin, L.-H. Hung, and A. P. Lee, "Droplet microfluidics," *Lab Chip*, vol. 8, pp. 198–220, 2008.

[12] J. Atencia and D. J. Beebe, "Controlled microfluidic interfaces," *Nature*, vol. 437, no. 7059, p. 648–655, 2004.

[13] A. Suea-Ngam, P. D. Howes, M. Srisa-Art, and A. J. deMello, "Droplet microfluidics: from proof-of-concept to real-world utility?," *Chem. Commun.*, vol. 55, pp. 9895–9903, 2019.

[14] H. Stone, A. Stroock, and A. Ajdari, "Engineering flows in small devices: Microfluidics toward a lab-on-a-chip," *Annu. Rev. Fluid Mech.*, vol. 36, pp. 381–411, 01 2004.

[15] T. Squires and S. Quake, "Microfluidics: Fluid physics at the nanoliter scale," *Reviews of Modern Physics*, vol. 77, p. 977, 10 2005.

[16] R. Malinowski, I. P. Parkin, and G. Volpe, "Advances towards programmable droplet transport on solid surfaces and its applications," *Chem. Soc. Rev.*, vol. 49, pp. 7879–7892, 2020.

[17] C. A. . C. M. Dong, L., "Lateral vibration of a water drop and its motion on a vibrating surface," *European Physical Journal*, vol. 21, p. 231–242, 12 2006.

[18] P. Goohpattader, S. Mettu, and M. Chaudhury, "Stochastic rolling of a rigid sphere in weak adhesive contact with a soft substrate," *The European Physical Journal E*, vol. 34, no. 11, pp. 1–11, 2011.

[19] S. Daniel, S. Sircar, J. Gliem, and M. Chaudhury, "Ratcheting motion of liquid drops on gradient surfaces †," *Langmuir : the ACS journal of surfaces and colloids*, vol. 20, pp. 4085–92, 06 2004.

[20] A. Buguin, F. Brochard, and P.-G. Gennes, "Motions induced by asymmetric vibrations: The solid/solid case," *The European physical journal. E, Soft matter*, vol. 19, pp. 31–6, 02 2006.

[21] S. Mettu and M. Chaudhury, "Motion of drops on a surface induced by thermal gradient and vibration," *Langmuir : the ACS journal of surfaces and colloids*, vol. 24, pp. 10833–7, 09 2008.

[22] X. Noblin, R. Kofman, and F. Celestini, "Ratchetlike motion of a shaken drop," *Physical review letters*, vol. 102, no. 19, p. 194504, 2009.

[23] R. Agapov, J. Boreyko, D. Briggs, B. Srijanto, S. Retterer, C. Collier, and N. Lavrik, "Length scale selects directionality of droplets on vibrating pillar ratchet," *Advanced Materials Interfaces*, vol. 1, 09 2014.

[24] S. K. D. W. D. M. Malvadkar NA, Hancock MJ, "An engineered anisotropic nanofilm with unidirectional wetting properties," *Nature Materials*, vol. 9, 2010.

[25] K. Sekeroglu and M. C. Demirel, "A fluidic device with polymeric textured ratchets," *Polymer*, vol. 58, pp. 30 – 35, 2015.

[26] N. Chamakos, G. Karapetsas, and A. Papathanasiou, "How asymmetric surfaces induce directional droplet motion," *Colloids and Surfaces A: Physicochemical and Engineering Aspects*, vol. 511, 09 2016.

[27] N. Tretyakov and M. Muller, "Directed transport of polymer drops on vibrating superhydrophobic substrates: A molecular dynamics study," *Soft matter*, vol. 10, 05 2014.

[28] S. Daniel, S. Sircar, J. Gliem, and M. K. Chaudhury, "Ratcheting motion of liquid drops on gradient surfaces," *Langmuir*, vol. 20, no. 10, pp. 4085–4092, 2004. PMID: 15969401.

[29] A. Shastry, M. J. Case, and K. F. Böringer, "Directing droplets using microstructured surfaces," *Langmuir*, vol. 22, no. 14, pp. 6161–6167, 2006. PMID: 16800671.

[30] T. A. Duncombe, E. Y. Erdem, A. Shastry, R. Baskaran, and K. F. Bohringer, "Controlling liquid drops with texture ratchets," *Advanced Materials*, vol. 24, no. 12, pp. 1545–1550, 2012.

[31] D. Caballero, J. Katuri, J. Samitier, and S. Sánchez, "Motion in microfluidic ratchets," *Lab Chip*, vol. 16, pp. 4477–4481, 2016.

[32] Y. Dong, H. R. Holmes, and K. F. Böhringer, "Converting vertical vibration of anisotropic ratchet conveyors into horizontal droplet motion," *Langmuir*, vol. 33, no. 40, p. 10745–10752, 2017.

[33] M. Bastopcu, A. Derinoz, A. C. Yilmaz, and E. Y. Erdem, "Textured surfaces as a new platform for nanoparticle synthesis," *Soft Matter*, vol. 14, pp. 4311–4316, 2018.

[34] N. Tretyakov and M. Müller, "Directed transport of polymer drops on vibrating superhydrophobic substrates: a molecular dynamics study," *Soft Matter*, vol. 10, pp. 4373–4386, 2014.

[35] H. Ding, X. Zhu, P. Gao, and X.-Y. Lu, "Ratchet mechanism of drops climbing a vibrated oblique plate," *Journal of Fluid Mechanics*, vol. 835, p. R1, 2018.

[36] E. Yelekli, *Oil droplet manipulation on superomniphobic textured surfaces.* PhD thesis, Bilkent University, 2020.

[37] P.-G. Gennes, F. Brochard-Wyart, D. Quéré, A. Reisinger, and B. Widom, "Capillarity and wetting phenomena: Drops, bubbles, pearls, waves," *Physics Today - PHYS TODAY*, vol. 57, pp. 66–67, 12 2004.

[38] M. Prakash, D. Quere, and J. Bush, "Surface tension transport of prey by feeding shorebirds: The capillary ratchet," *Science (New York, N.Y.)*, vol. 320, pp. 931–4, 06 2008.

[39] Y. Zheng, H. Bai, Z. Huang, X. Tian, F.-Q. Nie, Y. Zhao, J. Zhai, and L. Jiang, "Directional water collection on wetted spider silk," *Nature*, vol. 463, pp. 640–3, 02 2010.

[40] K. Liu, X. Yao, and L. Jiang, "Recent developments in bio-inspired special wettability," *Chem. Soc. Rev.*, vol. 39, pp. 3240–3255, 2010.

[41] "An essay on performance-reproduction," *Philos Sport Phys Educ.*, vol. 39, pp. 39–55, 1995.

[42] K. F. B. Ashutosh Shastry, Marianne J Case, "Directing droplets using microstructured surfaces," *Langmuir*, vol. 14, 7 2006.

[43] A. S. R. B. K. F. B. Todd A. Duncombe, E. Yegân Erdem, "Microfluidics: Controlling liquid drops with texture ratchets (adv. mater. 12/2012)," *Advanced Materials*, vol. 24, pp. 1497–1497, 03 2012.

[44] G. R. B. E. R. B. P. A. H. i. t. V. Álvaro G. Marín, Daniel Arnaldo del Cerro and D. Lohse, "Capillary droplets on leidenfrost micro-ratchets," *Physics of Fluids*, vol. 24, 12 2012.

[45] Y. Z. Jihua Zhang, Zhongjun Cheng and L. Jiang, "Ratchet-induced anisotropic behavior of superparamagnetic microdroplet," *Applied Physics Letters*, vol. 94, 4 2009.

[46] C. C. . D. Q. Guillaume Lagubeau, Marie Le Merrer, "Leidenfrost on a ratchet," *Nature Physics*, vol. 7, p. 395–398, 2011.

[47] A. A. Shukri, E. Erdem, R. Baskaran, and K. Böhringer, "Ratchet surface droplet transportation,"

[48] U. D. Koray Sekeroglu, Umut A. Gurkan and M. C. Demirel, "Transport of a soft cargo on a nanoscale ratchet," *Applied Physics Letter*, vol. 99, 2011.

[49] N. Tretyakov and M. Müller, "Directed transport of polymer drops on vibrating superhydrophobic substrates: a molecular dynamics study," *Soft matter*, vol. 10, no. 24, pp. 4373–4386, 2014.

[50] Ç. Varel and K. F. Böhringer, "Liquid droplet micro-bearings on directional circular surface ratchets," in *2014 IEEE 27th International Conference on Micro Electro Mechanical Systems (MEMS)*, pp. 983–986, IEEE, 2014.

[51] H. R. Holmes, A. E. Gomez, and K. F. Böhringer, "Timing and synchronization of droplets on ratchet conveyors," in *2016 IEEE 29th International Conference on Micro Electro Mechanical Systems (MEMS)*, pp. 796–799, IEEE, 2016.

[52] Y. Dong, H. R. Holmes, and K. F. Bohringer, "Converting vertical vibration of anisotropic ratchet conveyors into horizontal droplet motion," *Langmuir*, vol. 33, no. 40, pp. 10745–10752, 2017.

[53] Y. Dan, P. Xu, W. Zhang, and Z. Tan, "Improved genetic algorithm for parameters identification of cart-double pendulum," *Journal of Vibroengineering*, vol. 21, 07 2019.

[54] J. C. Sartorelli and W. Lacarbonara, "Parametric resonances in a base-excited double pendulum," *Nonlinear dynamics*, vol. 69, no. 4, pp. 1679–1692, 2012.

[55] I. M. Arkhipova, A. Luongo, and A. P. Seyranian, "Vibrational stabilization of the upright statically unstable position of a double pendulum," *Journal of sound and vibration*, vol. 331, no. 2, pp. 457–469, 2012.

[56] H. R. Holmes and K. F. Böhringer, "Transport velocity of droplets on ratchet conveyors," *Advances in colloid and interface science*, vol. 255, pp. 18–25, 2018.

[57] M. Naji, E. Yelekli Kirici, A. Javili, and E. Y. Erdem, "Describing droplet motion on surface-textured ratchet tracks with an inverted double pendulum model," *Langmuir*, vol. 37, no. 16, pp. 4810–4816, 2021.

[58] P. Xu, Y. Dan, W. Zhang, and Z. Tan, "Improved genetic algorithm for parameters identification of cart-double pendulum," *Journal of Vibroengineering*, vol. 21, no. 6, p. 1587–1599, 2019.

[59] M. Lampart and J. Zapoměl, "Dynamical properties of a nonautonomous double pendulum model," *Mathematical Methods in the Applied Sciences*, vol. 41, no. 17, pp. 7106–7114, 2018.

[60] O. Boubaker, "The inverted pendulum benchmark in nonlinear control theory: A survey," *International Journal of Advanced Robotic Systems*, vol. 10, no. 5, p. 233, 2013.

[61] C. Dorrer and J. Rühe, "Advancing and receding motion of droplets on ultrahydrophobic post surfaces," *Langmuir*, vol. 22, pp. 7652–7657, 08 2006.

[62] S. Khatoon, D. K. Chaturvedi, N. Hasan, and M. Istiyaque, "Optimal control of a double inverted pendulum by linearization technique," in *2017 International Conference on Multimedia, Signal Processing and Communication Technologies (IMPACT)*, pp. 123–127, 2017.

[63] U. ONEN, A. ÇAKAN, and I. ILHAN, "Performance comparison of optimization algorithms in lqr controller design for a nonlinear system," *Turkish Journal of Electrical Engineering & Computer Sciences*, vol. 27, no. 3, pp. 1938–1953, 2019.

[64] B. Aronov, S. Har-Peled, C. Knauer, Y. Wang, and C. Wenk, *Fréchet Distance for Curves, Revisited*, p. 52–63. MultiMedia Modeling, 2006.